Int J Adv Manuf Technol (2010) 46:43–50
DOI 10.1007/s00170-009-2064-1

ORIGINAL ARTICLE

Study on mechanism of chip formation during high-speed milling of alloy cast iron

Y. Yang · J. F. Li

Received: 23 November 2008 / Accepted: 15 April 2009 / Published online: 2 May 2009

Abstract By adopting an equivalent geometry model of chip, a finite element model was developed to study the mechanism of chip formation during high-speed milling of alloy cast iron. Several key technologies such as material constitutive model, friction model, chip separation criteria, chip damage criteria, heat dissipation, and transfer were implemented to improve the accuracy of finite element simulation. Saw-tooth chip of alloy cast iron was observed. The chip shape and cutting force agreed well with experimental results. The simulation results show that the maximum cutting temperature produced with appearance of saw-tooth chip crack, and it is located on the chip-tool contact surface. The saw-tooth chip is caused by double actions of thermoplastic instability and plastic instability. The chip saw-tooth degree decreases when increasing the rotating speed, while it increases when increasing the feed speed. This work provides a useful understanding for chip formation process and helps to optimize machining parameters and process of high-speed milling of alloy cast iron.

Keywords High-speed milling · Alloy cast iron · Saw-tooth chip · Chip formation mechanism · Finite element simulation

1 Introduction

As a result of the advances in machine tools and cutting tool technology, "high-speed milling (HSM)" became a cost-effective manufacturing process to produce parts with high precision and surface quality [1]. Recently, HSM has been employed for machining alloy cast iron and steels in hardened state (usually hardness >30 HRC) for making dies/molds used in the production of a wide range of automotive and electronic components, as well as plastic molding parts [2]. Machining of alloy cast iron at high cutting speeds is a cost-effective technology using advanced machine tools and cutting tools and offers several advantages such as reduction of finishing operations, elimination of distortion if the part is finish-machined after heat treatment, achievement of high metal removal rates, lower machining costs, and improved surface integrity [3, 4]. However, high-speed cutting of alloy cast iron results in high temperatures and stresses at the workpiece–tool interface. Consequently, cost-effective application of this technology requires a fundamental understanding of the machining process and the relationships between process variables on one hand and tool life and machined surface integrity on the other hand.

In machining hard materials, continuous chip formation is observed at conventional cutting speed and low feed rate. However, at higher cutting speed and feed rate, "saw-tooth" chips are produced [5]. The latter type of chip formation can cause periodical variations of both cutting and thrust forces and result in high-frequency vibrations [6]. In many papers dealing with cutting operations, the aim usually declared was to study the chip morphology by considering working parameters and physical properties of the machined material. Mabrouki [7] pointed out that chip morphology was affected by working parameters and machined material hardness. Albrecht [8] carried out a parametric study in order to study the phenomena accompanying saw-tooth chip formation. Ohbuchi [9] had studied chip formation in the domain of negative angle by introducing a stagnant region at the tool tip. The above

Y. Yang (✉) · J. F. Li
School of Mechanical Engineering, Shandong University, Jinan 250061, China
e-mail: yangyong913@gmail.com

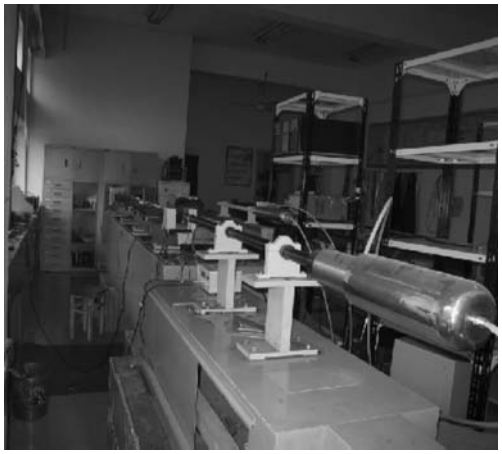

Fig. 1 SHPB experiment system

studies of chip morphology were not an objective in itself. The main objective was to explain the effects of chip morphology, on the one hand, on the workpiece in terms of machined surface integrity and, on the other hand, on tool wear behavior. In other words, the aim was to improve production efficiency. Recently, El-Wardany [10] presented an experimental investigation of chip formation mechanism during machining of tool steel with PCBN tools. Komanduri [11] studied the titanium chip morphology during cutting process and showed the saw-tooth chip formation was due to plastic instability. Barry [12] studied the mechanism of chip formation in machining hardened steels and concluded that the primary instability was the initiation of adiabatic shear at the tool tip and its propagation partway to the free surface of the workpiece material. However, for alloy cast iron, the chip formation process and mechanism during high-speed milling process are not yet well understood.

High-speed milling process can be better observed using finite element simulation. This method is emerging as useful techniques for explaining the observed phenomena in machining process. In this paper, FEM-based simulation was used to study the mechanism of chip formation during high-speed milling of alloy cast iron, and the influence laws of machining parameters on saw-tooth chip formation were also analyzed and discussed.

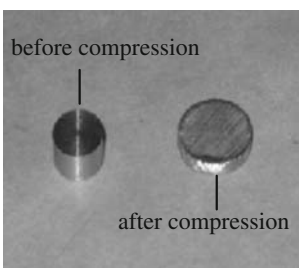

Fig. 2 Cylinder specimen

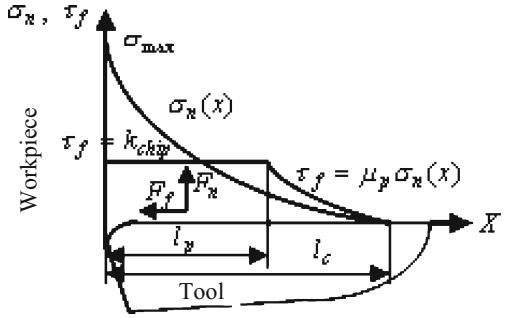

Fig. 3 Normal and frictional shear stress distribution at the chip–tool interface

2 Key technologies of finite element simulation

2.1 Material constitutive model

The material was modeled as isotropic elastic-plastic, with isotropic strain hardening. In the cutting processes, the deformation of the material in the cutting zone takes place at elevated temperature and high strains and strain rates. Therefore, in order to allow for their effect on the material properties, the flow stress of the material is taken as a function of strain, strain rate, and temperature using the Johnson–Cook constitutive equation taken from the [13]:

$$\sigma = [A + B(\varepsilon)^n]\left[1 + C\ln\frac{\dot{\varepsilon}}{\dot{\varepsilon}_0}\right] \times \left[1 - \left(\frac{T - T_{\text{room}}}{T_{\text{melt}} - T_{\text{room}}}\right)^m\right] \quad (1)$$

where σ is the flow stress (MPa), ε is the strain, $\dot{\varepsilon}$ is the strain rate (s^{-1}), $\dot{\varepsilon}_0$ is the reference strain rate (s^{-1}), T is the temperature (°C), T_{melt} is the material melting point, T_{room} is the room temperature, and A, B, C, n, m are the material parameters.

A Hopkinson apparatus was constructed to measure the flow stress at different strain rate and temperature for alloy cast iron. The Johnson–Cook constitutive equation was determined with these material data. The SHPB experiment system and specimen were illustrated in Figs. 1 and 2.

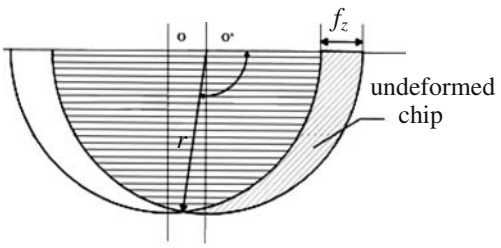

Fig. 4 Sketch of undeformed chip between two toolpasses with consideration of rotation of tool

The temperature in SHPB experiment was designed as 20°C, 100°C, 200°C, 300°C, and 500°C. The strain rate was designed as 500, 1,000, 3,000, 5,000, and 8,000 s^{-1}. According to the experiment result, the material parameters were calculated, and the J-C constitutive equation was determined. The value of A, B, C, n, and m were 522 MPa, 540 MPa, 0.0054, 0.3, and 1.15, respectively. Using the Johnson–Cook constitutive equation, finite element simulation of high-speed milling of alloy cast iron was carried out.

2.2 Friction model on the chip–tool interface

To obtain a reliable and realistic simulation result of metal cutting, it is essential to investigate the interaction between the cutting tool and the chip. The friction force is strongly influenced by cutting speed, contact pressure, and cutting temperature. Zorev's model revealed two distinct regions on the chip–tool interface sliding region and sticking region [14]. The normal and frictional shear stress distribution at the chip–tool interface was shown in Fig. 3.

From the tip of the tool up to a point, frictional stress was considered constant in a sticking region. After this point, frictional stress decreased on the tool rake face in a sliding region where Coulomb's friction law could be used. This can be represented as follows:

$$\tau_f = \mu\sigma_n, \text{ when } \mu\sigma_n < k_{chip}(\text{sliding}) \tag{2}$$

$$\tau_f = k, \text{ when } \mu\sigma_n \geq k_{chip}(\text{sticking}) \tag{3}$$

where τ_f is the frictional stress, σ_n is the normal stress, μ is the coefficient of friction, k is constant, and k_{chip} is the shear stress of the chip material.

The friction stress in the sticking region and constant friction coefficient μ in the sliding region can be obtained from the friction model. The friction coefficient is defined as follows:

$$\mu = F_f/F_n \tag{4}$$

$$F_f = F_c\sin\alpha + F_t\cos\alpha \tag{5}$$

$$F_n = F_c\cos\alpha - F_t\sin\alpha \tag{6}$$

Where F_f is the friction force on the tool rake face, F_n is the normal force on the tool rake face, α is the rake angle of cutting tool, F_c is the cutting force, and F_t is thrust force.

2.3 Chip separation criteria

Chip separation is achieved through a nodal release procedure in finite element code. This is done by defining a bonded interface along the cutting path and by applying a critical stress separation criterion to the stress state at a fixed distance ahead of the tool tip. When the stress state at the specified distance reaches a critical combination, the pair of bonded nodes just ahead of the tool tip will be released, resulting in chip separation from the workpiece. Specifically, the critical stress criterion refers to the attainment of a critical value of 1.0 by the stress index [15]:

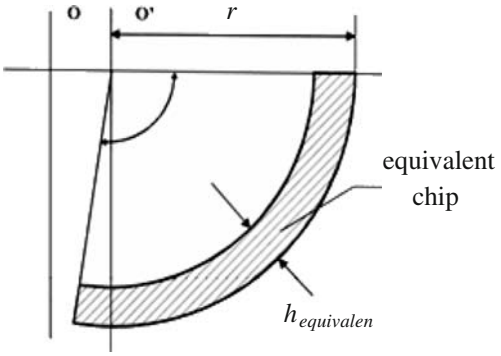

Fig. 5 Equivalent machining layer with constant thickness

$$f = \sqrt{(\sigma_n/\sigma_f)^2 + (\tau_n/\tau_f)^2} \tag{7}$$

where σ_n equals the normal stress when it is tensile and is set to zero when it is compressive, τ_n is the shear stress, and σ_f and τ_f are the material failure stress under pure tensile and shear loading conditions, respectively.

2.4 Chip damage criteria

The Cockroft and Latham damage criteria [16] had been used. The damage was evaluated according to the equation:

$$\int_0^{\varepsilon_f} \overline{\sigma}\left(\frac{\sigma^*}{\overline{\sigma}}\right)\mathrm{d}\overline{\varepsilon} = C \tag{8}$$

where C is the critical damage value given by a uniaxial tensile test, τ_f is the strain at the breaking condition, $\overline{\varepsilon}$ is the effective strain, $\overline{\sigma}$ is the effective stress, and σ^* is the maximum stress.

The criteria predict the material damage when the critical value C is exceeded. To optimize the material fracture in

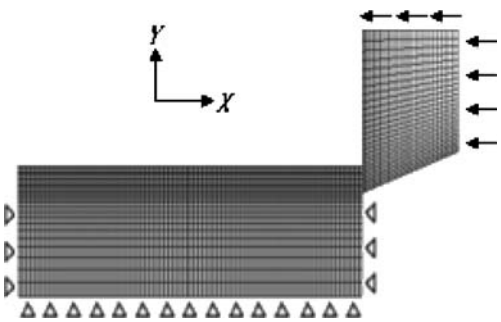

Fig. 6 Orthogonal finite element model

Table 1 Simulation and experiment cutting conditions

Number	Parameters			
	Rotating speed (rpm)	Feed per tooth (mm)	Depth of cut (mm)	Width of cut (mm)
1	5,000	0.04	0.3	0.3
2	6,000	0.04	0.3	0.3
3	8,000	0.04	0.3	0.3
4	10,000	0.04	0.3	0.3

cutting operations, a combined criterion has been used. The Cockroft and Latham criterion has been combined with a criterion based on the effective stress.

Two critical values have been defined, C and σ^*. The damage is evaluated for each element of the workpiece. The element deletion occurs when both the damage values are satisfied.

2.5 Heat dissipation and transfer

Knowledge of the temperature distribution in the workpiece, chip, and tool is very important since it has a great effect on the quality of the surface integrity and the tool wear. The main sources of heating, responsible for the high temperature rise observed in cutting processes, are the plastic work and the friction at the chip–tool interface, which are converted into heat. During high-speed machining, heat generated due to local energy dissipation does not have sufficient time to diffuse away, and local heating will occur in the active plastic zones and along the sliding frictional interface. Thus, temperature rise in the chip can be approximated with the adiabatic heating condition.

Machining is performed at ambient temperature (i.e., the initial temperature of both the workpiece and the tool is 20° C), while the heat losses to the environment from the free surface of the workpiece, due to convection heat transfer, are determined by the distributed heat flux:

$$q = h(T_W - T_O) \tag{9}$$

where h is the convection heat-transfer coefficient of the workpiece material, T_w is the temperature of the workpiece, and T_o is the ambient temperature, taken as 20°C. Heat transfer by radiation is considered insignificant and is not therefore taken into account.

3 Finite element model set-up and validation

3.1 Finite element model set-up

In the actual milling operation, the tip of the cutting edge travels on a trochoidal path due to the feed rate and spindle rotation. However, this path can be assumed to be circular for small values of feed per tooth (f_z). Thus, only rotational motion of the tool at a given spindle speed was considered in the process model (Fig. 4). Although the thickness of machining layer is variable continuously, for f_z is very small, it can be approximated using a circular element that has the equivalent constant thickness determined from the area of undeformed chip cross-section. Figure 5 showed the equivalent machining layer with constant thickness.

The equivalent chip thickness ($h_{\text{equivalent}}$) can be represented as [17]:

$$h_{\text{equivalent}} = r - r\sqrt{\frac{\cos^{-1}\left(\frac{f_z}{2r}\right) - \sin\left[2\cos^{-1}\left(\frac{f_z}{2r}\right)\right]}{\pi - \cos^{-1}\left(\frac{f_z}{2r}\right)}} \tag{10}$$

where r is radius of the tool.

The equivalent constant thickness chip was simplified, and orthogonal finite element model was established. The

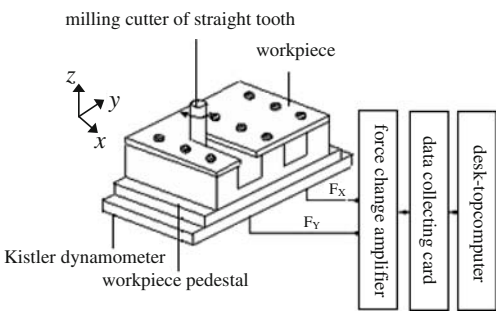

Fig. 7 Cutting force testing system

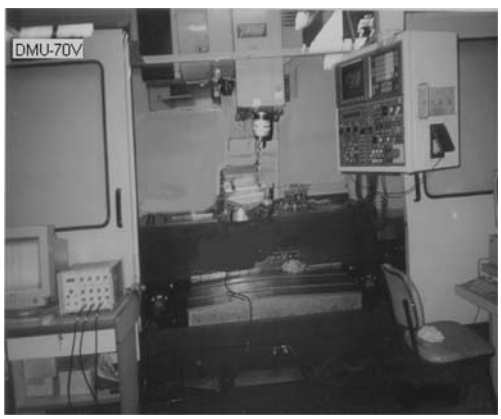

Fig. 8 Orthogonal experiment process

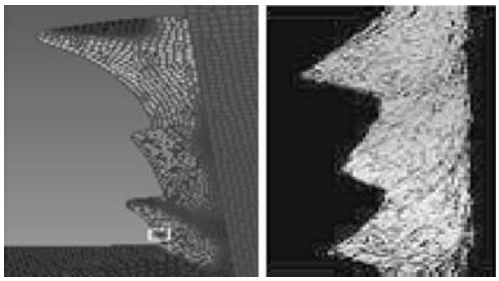

Fig. 9 Comparison of chip shape

dimensions and the initial finite element mesh of both the workpiece and the tool were shown in Fig. 6.

The workpiece element topology used was four-node isoparametric plane-strain quadrilateral elements. This kind of lower-order elements had been proven to be more accurate in analyzing large-strain plasticity problems. The tool element topology used was four-node isoparametric quadrilateral planar heat-transfer elements, as it was considered rigid and only heat-transfer analysis was carried out. Continuous adaptive remeshing is used to correct the problem of element distortion due to high deformations.

3.2 Finite element model validation

The workpiece material was Mo–Cr alloy cast iron (Cr, 0.25~0.35; Mo, 0.25~0.45), and the cutting tool material was a carbide with TiAlN coat. The material properties of workpiece and cutting tool were taken from the [18]. Different cutting speeds were used. The simulation and experiment cutting conditions were shown in Table 1. Making use of the finite element model, simulations of high-speed milling of alloy cast iron were performed with commercial code DEFORM.

To validate finite element simulation result, orthogonal milling experiments were conducted on a MV-5A numerical control machining center with cylindrical milling cutter of straight tooth (the diameter was 20 mm and had two teeth). The cutting force testing system was illustrated in Fig. 7, which consisted of Kistler9257A dynamometer, force charge amplifier, A/D data collecting card, and desk-top computer. The experiment process was illustrated in Fig. 8.

Table 2 Comparison of cutting forces

	Rotating speeds (rpm)			
	5,000	6,000	8,000	10,000
Predicted value (N)	68.08	65.5	59.62	57.84
Measured value (N)	61.5	57.76	53.32	50.62
Relative errors	10.7%	13.4%	11.8%	14.3%

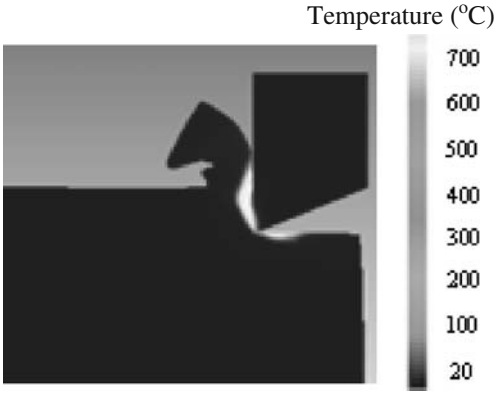

Fig. 10 Temperature distributions at rotating speed of 10,000 rpm

Comparison between simulation chip shape and experiment chip shape was shown in Fig. 9. As can be seen from Fig. 9, a good agreement was found.

Comparison between predicted and measured cutting forces were shown in Table 2.

The predicted cutting forces agreed well with the measured cutting forces. Relative errors of these two kind of cutting forces were less than 15%. The factors that cause the error were as follows: (1) There was difference between FEM material model and actual material properties in machining; (2) the tool was assumed as a rigid body and perfect sharp, but it was a hone radius edge in experiment and was an elastic-plastic body; (3) the thickness of undeformed chip, which was variable continuously in the experiment, was equivalent to a constant value in FEM. Considering the above assumptions and simplifications, the result of FEM was acceptable.

4 Chip formation process simulation and analysis

Orthogonal cutting simulations were performed at different cutting speed. The temperature and stress distribution during cutting process as well as the chip formation were predicted and analyzed.

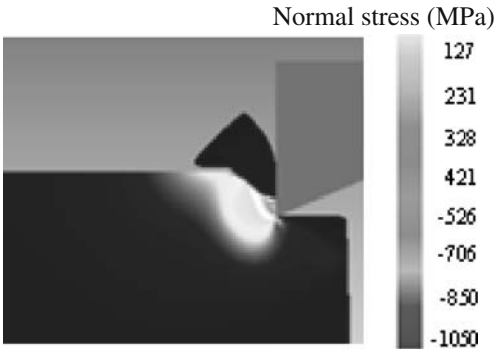

Fig. 11 Normal stress distributions at rotating speed of 10,000 rpm

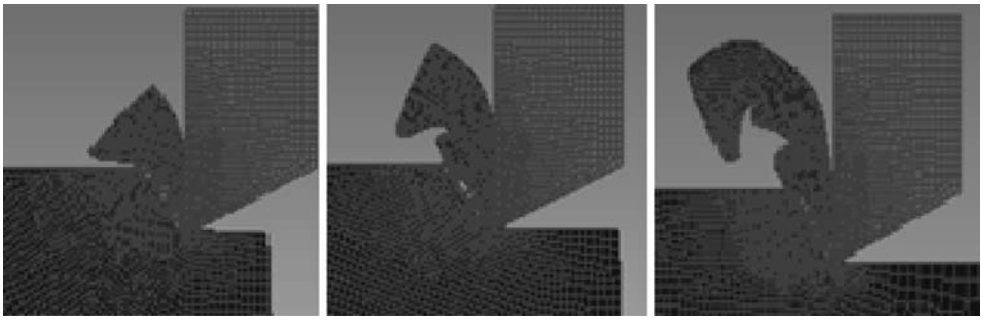

Fig. 12 Saw-tooth chip formation process of alloy cast iron at rotating speed of 10,000 rpm

4.1 Analysis of temperature and stress during cutting process

Figure 10 showed the temperature distribution on the chip–tool interface at rotating speed of 10,000 rpm. As can be seen in the figure, the maximum temperature produced with the appearance of saw-tooth chip crack. The maximum temperature was located on the chip–tool contact surface, and the temperature fell gradually when the crack extended.

Figure 11 showed the normal stress distribution of chip at rotating speed of 10,000 rpm. As seen in the figure, it was pressure stress on the contact surface between chip and tool rake face, while it was tensile stress far away from the contact surface. It was pressure stress inside the workpiece near the tool tip, and the pressure stress decreased gradually when deviating from the tool tip. It was tensile stress on the contact surface between chip and tool flank face, and the tensile stress decreased gradually when deviating from the contact surface.

4.2 Chip formation process and mechanism

The chip formation process of alloy cast iron at rotating speed of 10,000 rpm was illustrated in Fig. 12, and saw-tooth chip was observed during high-speed cutting process.

To study the saw-tooth chip formation mechanism, a chip segment formation process was observed in detail. The whole formation process of a chip segment was illustrated in Fig. 13 (the variable in the figure was equivalent stress).

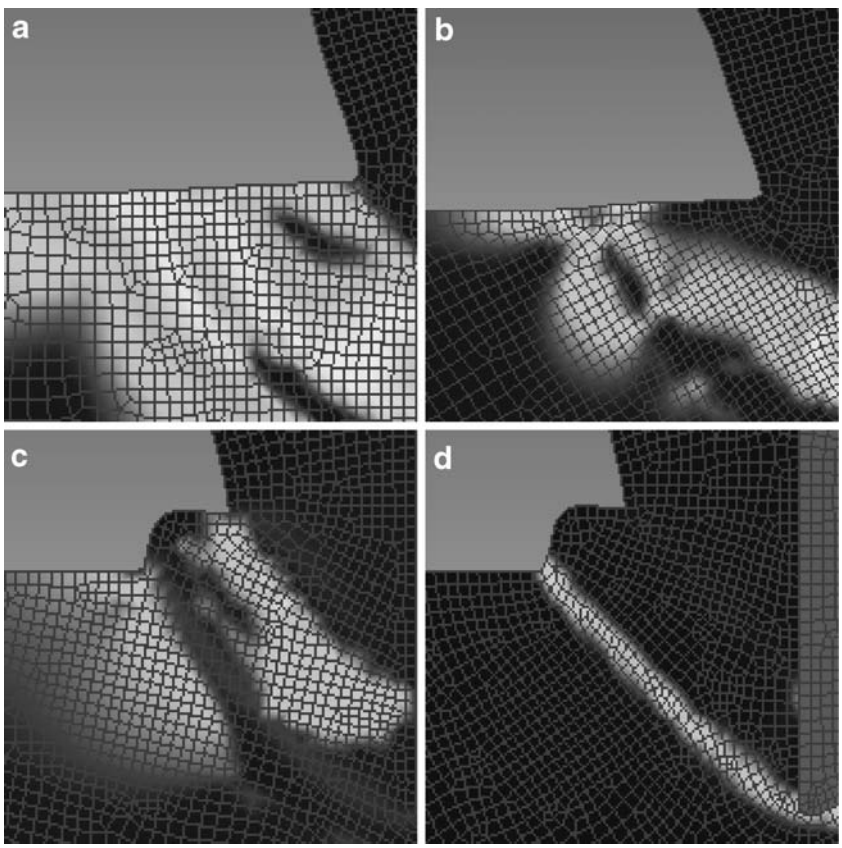

Fig. 13 The saw-tooth chip segment formation process at rotating speed of 10,000 rpm

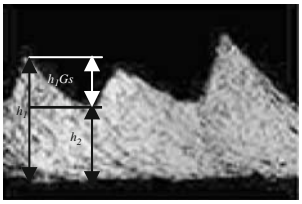

Fig. 14 The chip saw-tooth degree Gs

Figure 13a showed that the stress started localization at the workpiece surface. Figure 13b showed that the stress localization had formed, and the crack begins to appear at the workpiece surface. When the crack extended, it led to the formation of saw-tooth chip segment and is shown in Fig. 13c. Figure 13d showed the growth of chip segment at the same time the shear band appeared and formed gradually. Finally, the chip segment formed completely.

According to the chip segment formation process, the saw-tooth chip formation mechanism can be drawn: Alloy cast iron has the material character of high hardness and low heat conductivity. The cutting heat is difficult to emit due to the poor heat property and leads to the formation of shear band. Particularly, ahead of the tool tip, the local region is softened by the high temperature and results in the thermoplastic instability. On the other hand, stress localization caused by machining induration during cutting process leads to crack, and the crack extends together with the cutting process going along, resulting in the plastic instability. At last, the saw-tooth chip forms under double actions of thermoplastic instability and plastic instability. Therefore, it is can be said that the saw-tooth chip during high-speed cutting of alloy cast iron is caused by adiabatic shear and plastic fracture.

4.3 Influence laws of machining parameters on saw-tooth chip formation

The saw-tooth degree of chip can be denoted by the follow formula:

$$\mathrm{Gs} = (h_1 - h_2)/h_1 \tag{11}$$

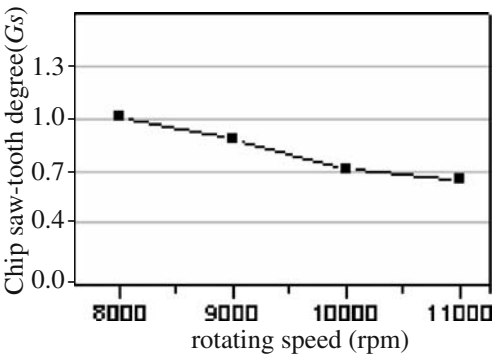

Fig. 15 Influence laws of rotating speed on saw-tooth chip formation

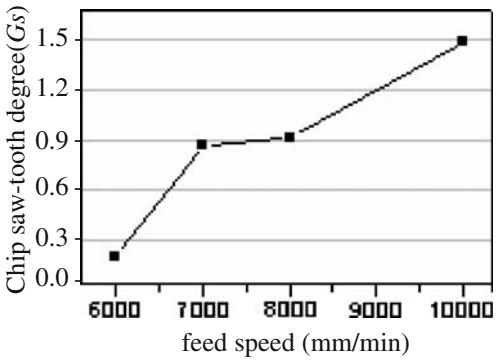

Fig. 16 Influence laws of feed speed on saw-tooth chip formation

where h_1 is the chip segment height, and h_2 is the chip root height.

Gs is described in Fig. 14.

At different cutting conditions, finite element simulations were performed, and the saw-tooth degree was calculated according to the predicted values of h_1 and h_2. Through analyzing saw-tooth degree of chip, the influence laws of machining parameters on saw-tooth chip formation can be drawn. Figure 15 showed the influence laws of rotating speed on saw-tooth chip formation, and Fig. 16 showed the influence laws of feed speed on saw-tooth chip formation.

As can be seen from the above figure, the chip saw-tooth degree Gs decreases when increasing rotating speed, while it increases when increasing feed speed. The influence laws curve of rotating speed on saw-tooth chip changes gently, while the influence laws curve of feed speed changes markedly, and it can be noted that the feed speed has great impact on chip saw-tooth degree.

The saw-tooth chip can lead to high-frequency periodic vibration of tool, making cutting force change periodically. As a result, the tool wear increases and the machining surface quality decreases. So, through the chip saw-tooth degree analysis and comparison, machining parameters optimization can be performed, and the tool life and machining surface quality can be improved.

5 Conclusions

The conclusions drawn are as follows:

1. Comparisons of predicted chip shape and cutting force with experimental results show that the finite element model developed in this paper is reasonable. The simulation results show that the maximum cutting temperature produced with appearance of saw-tooth chip crack. The chip saw-tooth degree decreases when increasing the rotating speed, while it increases when increasing the feed speed.

2. Temperature and stress distribution on the chip-tool interface are analyzed and studied, which is very difficult to measure by experiment.
3. The saw-tooth chip of alloy cast iron is caused by double actions of thermoplastic instability and plastic instability, which is a new point of view.
4. Further, the finite element model can be used to select optimal machining parameters and improve tool design, and excessive and expensive trial and error experiment process can be avoided.

Acknowledgments This work is supported by the National Natural Science Foundation of China (grant no. 50435020) and Postdoctoral Foundation of Shandong Province (grant no. 200703080).

References

1. Tlusty J (1993) High-speed machining. Ann CIRP 42(2):733–738. doi:10.1016/S0007-8506(07)62536-0
2. Dewes RC, Aspinwall DK (1997) A review of ultra high speed milling of hardened steels. J Mater Process Technol 69:1–17. doi:10.1016/S0924-0136(96)00042-8
3. Tönshoff HK, Bussmann W, Stanske C (1986) Requirements on Tools and Machines when Machining Hard Materials. Proc. of the 26th Int. Mach. Tool and Res. Conf 349-357
4. König W, Berktold A, Koch KF (1993) Turning versus grinding—a comparison of surface integrity aspects an attainable accuracies. Ann CIRP 42(1):39–43. doi:10.1016/S0007-8506(07)62387-7
5. Nakayama K (1974) The formation of saw tooth chips. Proc. Int. Conf. on Prod. Engr., Tokyo 572
6. Davies MA, Chou Y, Evans CJ (1996) On chip morphology, tool wear and cutting mechanics in finish hard turning. Ann CIRP 45 (1):77–82. doi:10.1016/S0007-8506(07)63020-0
7. Mabrouki T, Deshayes L, Ivester R, Rigal JF, Jurrens K (2004) Material modelling and experimental study of serrated chip morphology. In: Proceedings of the Seventh CIRP International Workshop on Model. Machin, Operation ENSAM Cluny (France)
8. Albrecht AB (1956) How to secure desired surface finish in turning operations. Am Mach 133–136
9. Ohbuchi Y, Obikawa T (2003) Finite element modeling of chip formation in the domain of negative rake angle cutting. Trans ASME J Eng Mater Techn 125:324–332. doi:10.1115/1.1590999
10. El-Wardany TI, Kishawy HA, Elbestawi MA (2000) Surface integrity of die material in high speed hard machining. Part 2. Microhardness variations and residual stresses. J Manuf Sci Eng 122:620–631. doi:10.1115/1.1286367
11. Komanduri R, Turkovich BF (1981) New observations on the mechanism of chip formation when machining titanium alloys. Wear 69:179–188. doi:10.1016/0043-1648(81)90242-8
12. Barry J, Gerald B (2002) The mechanisms of chip formation in machining hardened steels. Trans ASME J Manuf Sci Eng 124 (3):528–535. doi:10.1115/1.1455643
13. Johnson GR, Cook WH (1983) A constitutive model and data for metals subjected to large strains, high strain rates and high temperature. In: Proceedings of the Seventh International Symposium on Ballistics, The Haque, The Netherlands 541–547
14. Zorev NN (1963) Interrelationship between shear processes occurring along tool face and shear plane in metal cutting. International Research in Production Engineering 42–49
15. Hibbit D, Karlsson B, Sorenson P (1999) ABAQUS theory manual (ver 5.8). Hibbit, Karlsson & Sorenson, USA
16. Cockroft MG, Latham DJ (1966) A simple criterion of fracture for ductile metals. National Engineering Laboratory, UK Report 216
17. Dong HY, Ke YL (2005) Simulation of 3D chip shaping of aluminum alloy 7075 in milling processes. Trans Nonferrous Met Soc China 15(6):1315–1321
18. Yang Y, Li JF, Sun J (2008) Three-dimensional modeling and simulating of high-speed milling of alloy cast iron. Proceedings of First International Conference on Modeling and Simulation, Nanjing, P.R. China August 5–7, 231–236